Research Article

High photocatalytic performance of 3D porous-structured TiO_2@ natural rubber hybrid sheet on the removal of indigo carmine dye in water

Chaval Sriwong[1,2] · **Kittisak Choojun**[1,3] · **Sukanpirom Sriwong**[4]

Abstract

Due to the high efficiency of photocatalytic process for the environmental treatments, titanium dioxide (TiO_2) is a popular used as photocatalyst material. However, the practical uses of TiO_2 in powder form have some drawbacks as well as the difficult reusability. In this work, 3D porous-structured TiO_2@natural rubber (TNR) hybrid sheets with high photocatalytic performance were presented. TNR hybrid sheets prepared by a facile and low-cost method, which is based on the mixing of natural rubber (NR) latex (60% high ammonia) and ammoniacal TiO_2 (P25) suspension, followed by vacuum filtration through a sintered glass template to make a 3D porous network structure on the surface of the sheets. The obtained TNR sheet samples were characterized by scanning electron microscopy (SEM), energy dispersive X-ray spectrometer (EDX), X-ray diffractometer (XRD) and reflection Fourier transformed infrared spectroscopy (FT-IR) techniques. The results showed that the surface morphologies of TNR hybrid sheets appeared as porous-structured which had high roughness and with various tiny pores on the surface. The photocatalytic properties of the prepared TNR hybrid sheets were tested using indigo carmine (IC) dye under UV light irradiation. It was found that the highest photodegradation efficiency was achieved with the TNR_5 wt% hybrid sheet sample. Compared with the sheets reported in previous works, the TNR sheet shows higher efficiencies than those sheets due to its higher amount of TiO_2 particles at the surface, more porous structure with high rough surface, and abundance of tiny pores on the TNR sheet surface. Moreover, the recyclability and stability of TNR sheet indicated that upon using 10 cycles (remains 98% efficiency), in which the stability of the sheet surface well-confirmed by SEM and XRD techniques, as well. From above the study, this 3D porous-structured TNR hybrid sheet could be a new alternative strategy for the water or wastewater treatment in industry concerning with the easy use, recovery, reusability and stability of the photocatalysts.

Keywords Photocatalytic process · Titanium dioxide (TiO_2) · TiO_2-rubber sheet · 3D structure · Indigo carmine (IC)

Electronic supplementary material The online version of this article (https://doi.org/10.1007/s42452-019-0900-y) contains supplementary material, which is available to authorized users.

✉ Chaval Sriwong, chaval.sr@kmitl.ac.th | [1]Department of Chemistry, Faculty of Science, King Mongkut's Institute of Technology Ladkrabang, Chalongkrung Road, Ladkrabang, Bangkok 10520, Thailand. [2]Smart Materials Research and Innovation Unit, Faculty of Science, King Mongkut's Institute of Technology Ladkrabang, Chalongkrung Road, Ladkrabang, Bangkok 10520, Thailand. [3]Catalytic Chemistry Research Unit, Department of Chemistry, Faculty of Science, King Mongkut's Institute of Technology Ladkrabang, Chalongkrung Road, Ladkrabang, Bangkok 10520, Thailand. [4]Department of Chemical Engineering, Faculty of Engineering, King Mongkut's Institute of Technology Ladkrabang, Chalongkrung Road, Ladkrabang, Bangkok 10520, Thailand.

SN Applied Sciences (2019) 1:864 | https://doi.org/10.1007/s42452-019-0900-y

Received: 11 May 2019 / Accepted: 8 July 2019 / Published online: 17 July 2019

1 Introduction

In the past decades, the utilizations of photocatalyst materials for the environmental protection, purification and remediation have been of interest worldwide [22]. Particularly, the heterogeneous photocatalysis using semiconductors as catalysts has been considered as a cost-effective alternative treatment process for the dye removal containing in wastewaters [21]. Among all photocatalysts, titanium dioxide or titania (TiO_2) is the most widely used as a photocatalyst material because of its availability, low cost, non-toxicity, high stability and high activity in the photocatalysis process [8]. Currently, the commercially available TiO_2 powder, Degussa P25 shows the highest photoactivity. Thus, it is the most commonly used in many kinds of photocatalytic applications [23, 26]. However, there are some drawbacks by using TiO_2 in form of powders; for instance, [1] difficulty in the applying and reusing for continuous flow systems, [2] the limitation in separating the powder from the system at the end of the process, and [3] easy aggregation of TiO_2 particles in suspensions, especially at the high loading [2, 5]. To avoid these problems, many researchers have been tried to prepare or coat TiO_2 as films on the various substrates, such as, glass [15], ceramics [20], stainless steel [40] and wood [6]. Nevertheless, some of these substrates are expensive and have limitations in an application.

Due to the outstanding of several advantages of polymer substrates, such as, flexibility in nature, mechanical and chemical stabilities, high durability, low cost and availability [29]; hence, it has been used as a support for TiO_2 photocatalyst. Recently, various types of polymeric materials used as the polymer-supported TiO_2 have shown promising performance for the photocatalysis, for example, polyaniline (PANI) [18], polyethylene terephthalate (PET) [9], silicone [28], polymethyl methacrylate (PMMA) [7] and high-density polyethylene (HDPE) [14]. Though, the methods or techniques to prepare the polymer-supported TiO_2 photocatalyst, such as, sol–gel and spin coating [16], dip and spin coating [3, 4, 36] and plasma layer deposition [17], are practically difficult and still have some disadvantages. To overcome above obstacles, facile, cheap and high effective methods are still an interesting topic under investigation.

Recently, we have reported easy and economical methods for the preparation of the polymer-supported TiO_2 photocatalysts under the general name "TiO_2-rubber" sheets [31–34]. These methods are based on the use of natural rubber latex (natural hydrocarbon polymer) and commercially titania (Degussa P25) powder as starting materials. The obtained TiO_2-rubber composite sheets from various methodologies had different surface morphologies; therefore, they showed different photodegradation activities of organic dyes under UV light irradiation. Interestingly, furthermore, we found that they could be easily recovered after use and reused many times with no loss of efficiency and, in some case, with no need for the cleaning prior to the next time.

To continue our efforts on improving the TiO_2-rubber sheets, we herein report an extension of our work involving the three dimensional (3D) porous-structured TiO_2@natural rubber (TNR) hybrid sheets which had high TiO_2 particles content, roughness and porous network structured with tiny pores on the surface of sheets. To the best of our knowledge, moreover, none of the published research work has prepared as the 3D porous-structured TiO_2-rubber hybrid sheet using a sinter glass filter as an imprinted template to build 3D structure of TiO_2 nanoparticles impregnated on the surface of natural rubber substrate sheet. The results indicated that the as-prepared TNR hybrid sheet in this present work shows better activity on the photodegradation of indigo carmine (IC) dye in water under UV light irradiation than those the previously reported sheets. In addition, the recyclability and stability of the TNR hybrid sheet are investigated and also reported.

2 Experimental details

2.1 Materials and chemicals

Titanium dioxide (TiO_2) Degussa P25 (Anatase 80: Rutile 20) was supplied from Degussa AG, Germany. The natural rubber (NR) latex (60% HA, 60% dry rubber content, high ammonia (HA)) was obtained from Chana Latex Co. Ltd., Songkhla, Thailand. Ammonia solution (NH_4OH, 28–30%) was purchased from Baker, USA. Indigo carmine (IC) dye was purchased from Fluka, USA. All chemicals were used as received without further purification. The sintered glass filter (SGF) template (150 mL, F4–5.5 ASTM) has a pore size of 4–10 µm was supplied from PYREX®, USA.

2.2 Preparation of TNR hybrid sheets

In this work, TNR hybrid sheet samples were prepared by using a modified method from our previously reported [31] with the varying contents of NR latex with 5 wt%, 10 wt% and 15 wt%, respectively. The TNR sheet samples were labeled as TNR_*x* %, which *x* shows the natural rubber (NR) contents for the weight percentage (wt%) of NR to TiO_2. In the preparation of 3D porous-structured TNR_5 wt% sheet sample, about 0.84 mL of NR latex was mixed with 9.16 mL of distilled water under stirring for 5 min. In the separate flask, the ammoniacal TiO_2 suspension was prepared by

mixing 0.50 g of TiO_2 powder with 5 mL ammonia solution and vigorously stirred for 10 min. Then, the as-prepared 10 mL of diluted rubber latex was added to the TiO_2 suspension and continuously stirred for 10 min. Then, the mixture was subjected to vacuum suction through a sintered glass filter mold and dried in the oven at 60 °C about 3 h. After that, the sheet sample was carefully taken out from the sintered glass, and was turned upside down. It was left to dryness at room temperature overnight, and finally the TNR_5 wt% hybrid sheet was obtained. For comparison, the TNR_10 wt% and TNR_15 wt% sheet samples were also prepared likewise using appropriate amounts of natural rubber latex, 1.68 mL and 2.52 mL, respectively.

2.3 Methods of TNR hybrid sheets characterizations

The surface morphologies of all the TNR hybrid sheet samples were characterized by using a scanning electron microscopy (SEM) (Quanta 250, USA) attached with energy dispersive X-ray spectrometer (EDX) (Oxford ISIS 300, UK). The functional groups of natural rubber and TiO_2 were also investigated using a reflection Fourier-transformed infrared spectroscopy (FTIR) (Nicolet iS50, Thermo Fisher Scientific Inc., USA). The phases of natural rubber and TiO_2 were identified by X-ray diffractometer (XRD) (XRD-6100, Shimadzu, Japan).

2.4 Photocatalytic study of TNR hybrid sheets characterizations

The photocatalytic activities of all the obtained TNR hybrid sheets were evaluated by monitoring decolorization of IC dye in water (2.5×10^{-5} M) in a similar manner as been described previously [31]. The concentrations of IC dye samples after photodegradation were analyzed using a UV–Visible spectrophotometer (Evolution 201, Thermo Scientific, USA). The percentages of degradation efficiencies were calculated by Eq. (1),

$$\% \text{ Degradation efficiency} = \frac{C_0 - C_t}{C_0} \times 100 \quad (1)$$

where C_0 is the initial concentration of IC dye solution and C_t is the concentration at a specific time interval of the collected samples [25].

3 Results and discussion

3.1 SEM and EDX analysis of TNR hybrid sheets

The surface morphologies of all the obtained TNR hybrid sheets and the sintered glass filter (SGF) template were studied using SEM technique. The morphologies of the SGF template are shown in the Fig. 1a, b. For all the 3D porous-structured TNR hybrid sheet samples, the surface morphologies are like host–guest pair, especially for the TNR_5 wt% sheet (in Fig. 1c, d). The results of these are due to the fact that the surfaces of TNR hybrid sheets were imprinted by the contour morphology of the surface of sintered glass filter. The sintered glass filter used in this work acted as the "template or mold" out of which the 3D network and porous structures on the TNR hybrid sheets surface were made.

The SEM images of the surface morphologies of all as-prepared TNR sheet samples are shown in Fig. 2, and in Fig. S1 (at high magnification of 10,000×). It can be clearly observed that the different contents of rubber latex used in the preparation of TNR sheets directly affected on the surface morphology. The 3D porous network structure with roughness and the content of TiO_2 particles at the surface of TNR hybrid sheets decreased with the increasing amount of NR latex. Especially, the TNR_5 wt% hybrid sheet (in Fig. 2a, d) shows the highest near surface TiO_2 particles content with rough surface. Moreover, its well 3D porous network structured surface is full of tiny holes compared with the other two sheets. When using the higher content of NR latex, the hybrid sheet became thicker, denser and TiO_2 particles more readily submerged in the rubber matrix. These result in the less content of TiO_2 particles appeared on the surface of the sheets, as shown in Fig. 2f, e. The occurrence of porous structure with the tiny holes on the surface of TNR_5 wt% sheet (see in Fig. 2a, d) but not on the other two higher content of rubber latex sheets could due to the thinner layer of the sheet resulting the fully air flow during the vacuum suction step. The pores size of these tiny holes had diameter in the range of 0.5–1.5 µm, as seen in the red arrow inset of Fig. 2d (×_10,000 magnification).

The EDX analysis was carried out to investigate the presence of elements in the TNR hybrid sheets surface. For all samples, only three elements were detected in these sheets including carbon, oxygen and titanium atoms. Figure 3 displays the EDX mapping of TNR_5 wt% and TNR_15 wt% hybrid sheet samples. In comparison, the TNR_5 wt% sheet (see in Fig. 3a) shows more distribution of Ti (TiO_2 particles) atoms, but less carbon atoms of natural rubber latex (*cis*-1,4-polyisoprene) on the sheet surface than the TNR_15 wt% sheet (in Fig. 3b). This result corresponds to the SEM results shown in Fig. 2c and 2f, where there is a small amount of TiO_2 particles on the surface of high content rubber sheet.

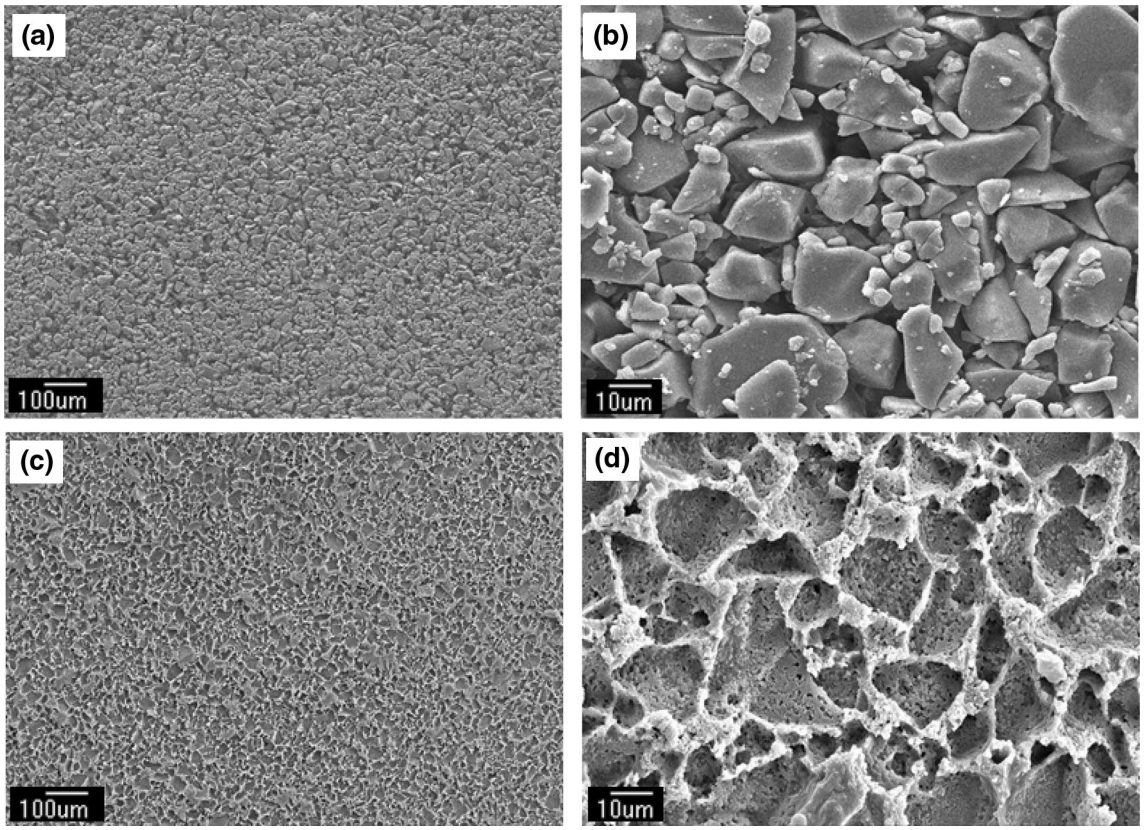

Fig. 1 SEM images of the surfaces of the sintered glass filter template: **a** low magnification_×100, **b** high magnification_×1000; and the obtained 3D porous-structured TNR hybrid sheet: **c** low magnification_×100, **d** high magnification_×1000

3.2 FT-IR analysis of TNR hybrid sheets

The functional groups of both TiO_2 and natural rubber were analyzed by FTIR spectroscopy technique. Figure 4 illustrates the FTIR spectra of pristine TiO_2 powder, pure natural rubber sheet, and all the prepared TNR hybrid sheet samples. From the Fig. 4a, the broad band spectrum below ~ 800 cm^{-1} corresponding to the characteristic vibrational mode of TiO_2 (Ti–O stretching mode of Ti–O–Ti) as observed in pristine TiO_2 powder [12]. The characteristic absorption peaks of polyisoprene structure (–CH_2CH_3C=$CHCH_2$–) appeared at ~ 3028 cm^{-1} for =C–H stretching, 2950 cm^{-1} for –CH_3 asymmetric stretching, 2914 and 2850 cm^{-1} for –CH_2 asymmetric and symmetric stretching, 1641 cm^{-1} for –C=C– stretching of isoprene group of rubber, 1440 cm^{-1} for –CH_2 deformation, 1373 cm^{-1} for –CH_3 deformation, 829 cm^{-1} for =C–H out of plane bending, and 569 cm^{-1} for –C–C–C– main chain deformation [1, 33], as shown in Fig. 4e. In addition, some extra absorption bands are observed around at 3500–3100 cm^{-1} corresponds to the stretching vibration modes of –O–H and –N–H groups in adsorbed water and ammonia molecules [11]. The FTIR spectra of the surface of 3D porous-structured TNR hybrid sheets are shown in Fig. 4b–d. All of the absorption bands of the sheets are those of the vibration modes of pristine TiO_2 and natural rubber indicating the hybrid of both TiO_2 particles and natural rubber. From these spectra, the band intensities of the natural rubber in TNR hybrid sheets at 2950, 2914, 2850, 1641 and 1440 cm^{-1} increased with the increasing amount of rubber latex (TNR_15 wt% > TNR_10 wt% > TNR_5 wt%). From this result, the TNR_15 wt% sheet having the highest content of natural rubber covered on the sheet surface; thus, it should have the lowest TiO_2 particles embedded on the sheet surface, which is in good agreement with SEM, EDX and XRD results. Furthermore, it is observed that the strong absorption peak around at 1641 cm^{-1} (–C=C– stretching) of natural rubber is shifted to higher wavenumber in the TNR hybrid sheets (1647, 1666 and 1668 cm^{-1} for the TNR_15 wt%, TNR_10 wt% and TNR_5 wt% sheets, respectively). This result may be ascribed to the induced interaction between TiO_2 nanoparticles and natural rubber by the formation of hydrogen bond between a proton-donor group (such as hydroxyls, Ti–OH) and a proton-acceptor group (such as double bonds, –CH_2CH_3C=$CHCH_2$–) [35].

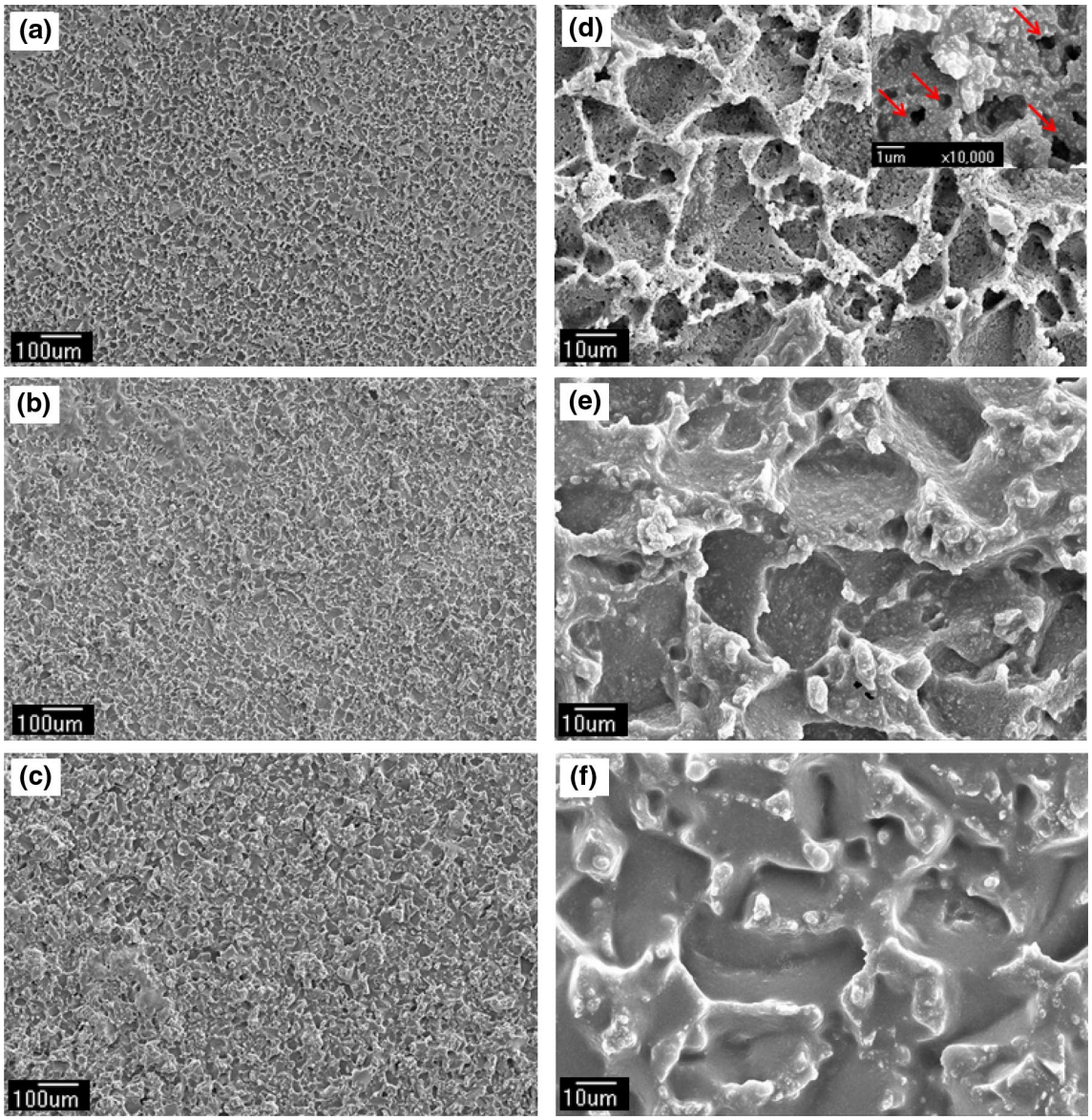

Fig. 2 SEM images of the surfaces of TNR hybrid sheets at low magnification_×100 (left column) and high magnification_×1000 (right column) of: 3D porous-structured TNR_5 wt% sheet (**a**, **d**), TNR_10 wt% sheet (**b**, **e**), and TNR_15 wt% sheet (**c**, **f**)

3.3 XRD characterization of TNR hybrid sheets

The X-ray diffraction patterns of pristine TiO_2 powder and the 3D porous-structured TNR hybrid sheet samples are shown in Fig. 5. The anatase characteristic peaks appear at $2\theta = 25.5°$, 37.9°, 48.1°, 53.9°, and 55.2° while those of rutile are at $2\theta = 27.5°$, 36.1°, and 54.50° [10, 37]. From this figure, the well crystallized of both anatase and rutile forms were observed in all the TNR hybrid sheets (in Fig. 5b–d) and were identical to those of commercial TiO_2 (Degussa P25) powder in Fig. 5a. In addition, a broad scattering peak around $2\theta = 19°$ of natural rubber matrix was discernible in the patterns of all the sheet samples. The XRD of pristine rubber sheet has been previously shown [31, 32] only a large broad peak near $2\theta = 19°$ since the rubber matrix is composed of low atomic number (low Z) elements. It noted that the relative intensities of this broad peak increase with increasing amount of rubber latex. The matrix of TNR_5 wt% sheet has the highest proportion of TiO_2 particles than those of the other sheets; therefore, the highest average Z-value of matrix in the former resulting in the lowest X-ray scattering and the lowest intensity peak at $2\theta = 19°$ as shown in Fig. 5b. This result indicated that the TNR_5 wt% sheet has the highest TiO_2 particles embedded and covered on the sheet surface than the other two

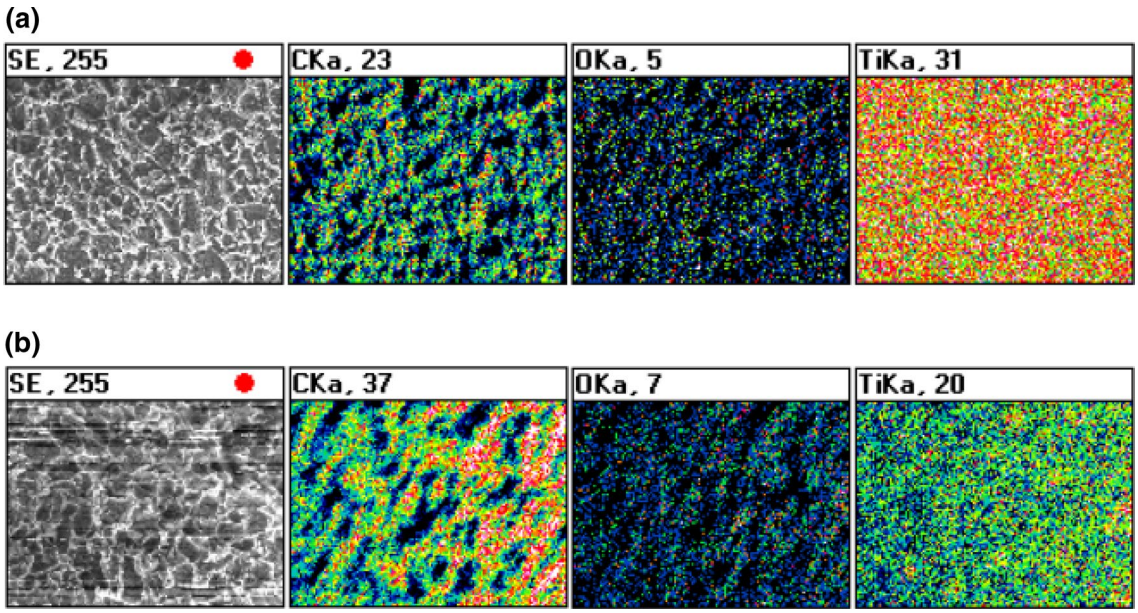

Fig. 3 EDS elemental mapping of (**a**) 3D porous-structured TNR_5 wt% and (**b**) TNR_15 wt% hybrid sheets

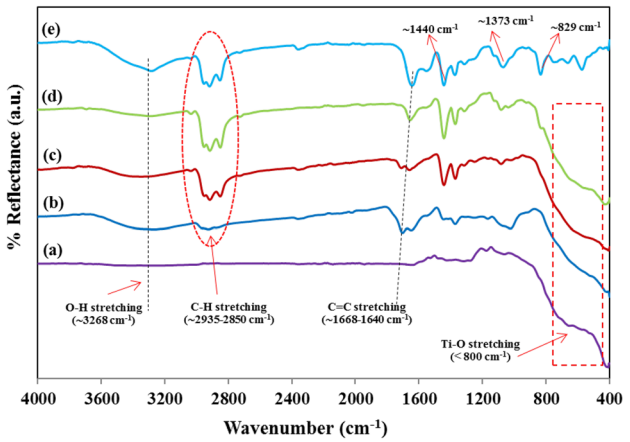

Fig. 4 FTIR spectra of (a) pristine TiO_2 (Degussa P25) powder; (b) 3D porous-structured TNR_5 wt%, (c) TNR_10 wt%, and (d) TNR_15 wt% hybrid sheets; and (e) pristine natural rubber (NR) sheet

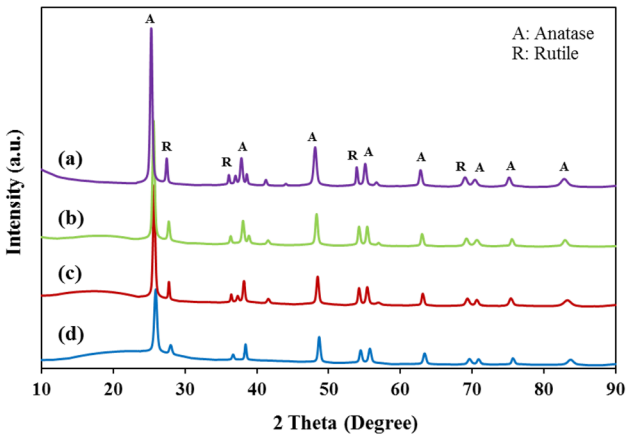

Fig. 5 XRD patterns of (a) pristine TiO_2 (Degussa P25) powder, and 3D porous-structured (b) TNR_5 wt%, (c) TNR_10 wt% and (d) TNR_15 wt% hybrid sheets

sheets, in which agreement with the results studied from SEM, EDS, and FTIR techniques.

3.4 Photocatalytic activities of TNR hybrid sheets

The photodegradation of IC dye solution by the 3D porous-structured TNR hybrid sheet samples under UV-light irradiation is shown in Fig. 6. It can be clearly seen that TNR_5 wt% sheet has the highest photocatalytic efficiency than that of the TNR_10 wt% and TNR_15 wt% sheets, respectively. As shown in Fig. 2a, d, the TNR_5 wt% sheet has the highest near surface TiO_2 particles content, rough surface, and 3D porous network structured with the tiny holes; therefore, it has the highest photocatalytic activity than the other two sheets. Normally, it is well-known that the photocatalytic activity on the TiO_2 surface is very sensitive to its surface structure and roughness because this type of photocatalysis is a surface reaction [15, 22, 38]. Thus, the larger the surface structure with high porous surface as well as surface roughness, the more the photocatalytic reaction will take place. On the other hand, the lower the porous surface morphology and surface roughness as in the smooth surface sheet will have lower photodegradation activity.

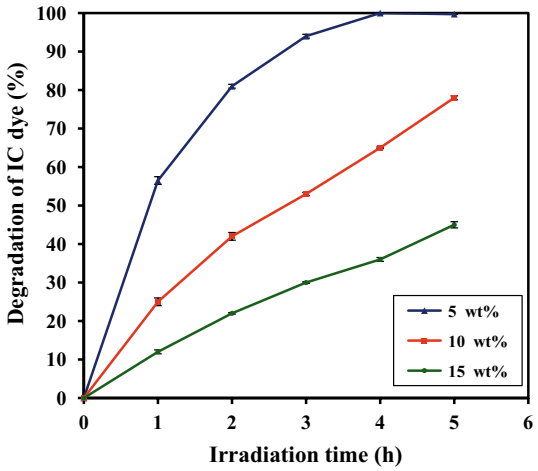

Fig. 6 Efficiencies of photocatalytic degradation of IC dye solution using 3D porous-structured TNR hybrid sheet samples under UV irradiation

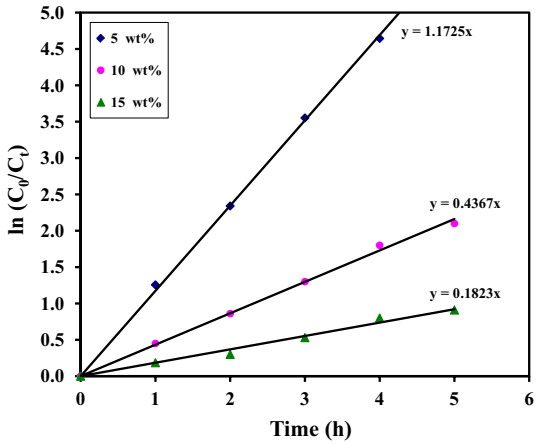

Fig. 7 Plots of the reaction kinetics on the photocatalytic degradation of IC dye solution using 3D porous-structured TNR hybrid sheet samples under UV irradiation

The reaction kinetic of the photodegradation of IC dye solution by 3D porous-structured TNR hybrid sheets was also studied. The apparent rate constant ($k_{app.}$) has been chosen as the basic kinetics parameter for all the TNR sheet samples. The apparent rate constant was obtained from the Langmuir–Hinshelwood pseudo first-order kinetics equation as:

$$\ln\left(\frac{C_0}{C}\right) = k_{app.} \times t, \tag{2}$$

where C_0 is the initial concentration of IC dye solution, C is the concentration at time (t), and $k_{app.}$ is the apparent rate constant. The results yielded straight lines as shown in Fig. 7 confirmed the pseudo first-order kinetic reaction [13, 24, 39] in IC dye of the photodegradation process with the rate constants were 1.1725 h^{-1}, 0.4367 h^{-1} and 0.1823 h^{-1} for the TNR_5 wt%, TNR_10 wt% and TNR_15 wt% sheets, respectively. Moreover, the efficiency of this 3D porous-structured TNR_5 wt% hybrid sheet was also compared with sheets of the same type previously reported from our group [30–32]. These sheets though prepared by different methods but they all employed the same starting materials (TiO_2 (Degussa P25) and natural rubber latex 60% HA). The rate constant values of each catalyst sheet are summarized in Table 1, where the rate constant ($k_{app.}$) of TNR hybrid sheet in this work is the highest one. The best performance observed in the TNR sheet can be traced back to its relatively higher content of TiO_2 at the surface, roughness, porosity, and 3D network structured with tiny holes on the sheet surface (see in Fig. S2), causing the enhancement of the photocatalytic activity of TNR hybrid sheet. The rough surface and the porous structure are very important for the photocatalytic activity of TiO_2 films [3, 4, 24], thus when these conditions are met the system usually performs at its best. In addition, the possibility of the photocatalytic reaction process could be proposed, which as illustrated in Fig. 8. In brief, when TNR sheet surface were irradiated by UV light, the electron–hole pairs of TiO_2 nanoparticles were generated that the electrons were excited from the valence band (VB) to the conduction band (CB) [Eq. (3)]. Then, electrons (e^-) in the CB reacted with oxygen (O_2) to produce superoxide anion radical ($O_2^{\circ-}$) [Eq. (4)], whereas the positive holes (h^+) left in the VB reacted with the hydroxide ion (OH^-) or water (H_2O) to generate hydroxyl radicals (OH°) [Eq. (5)]. The strongly reactive OH° radicals then reacted with the IC dye molecules and initiated the dye degradation process, resulting in the harmless final products, such as, carbon dioxide (CO_2), water, and some ions [Eq. (7)] [19, 27].

$$\text{TNR sheet}\left(TiO_2\right) + h\nu \rightarrow h^+ + e^- \tag{3}$$

$$O_2 + e^- \rightarrow O_2^{\circ-} \tag{4}$$

Table 1 Rate constant values on the photocatalytic degradation of IC dye solution under UV light over 3D porous-structured TNR hybrid sheet and the other sheets

Sample	Rate constant, $k_{app.}$ (h^{-1})	R^2	References
Imp-25 sheet	0.5447	0.9892	Sriwong et al. [30]
FT-sheet	0.8247	0.9877	Sriwong et al. [31]
TiO_2-strewn sheet	0.9138	0.9810	Sriwong et al. [32]
TNR hybrid sheet	1.1725	0.9931	This work

The photocatalytic study of all sheets were investigated under the same conditions (dye concentration, intensity of UV light; see in the experimental section of each reference)

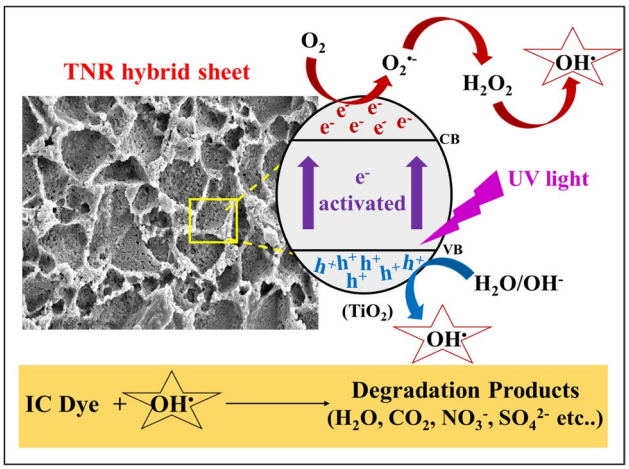

Fig. 8 Proposed the photocatalytic reaction process of 3D porous-structured TNR hybrid sheet on the degradation of IC dye under UV light irradiation

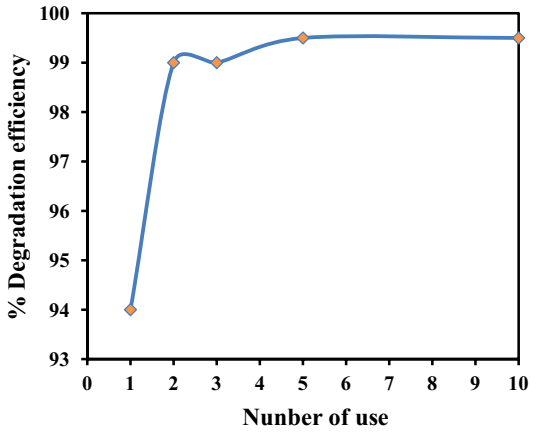

Fig. 9 The efficiencies of IC dye photodegradation by 3D porous-structured TNR_5 wt% hybrid sheet after repeated uses (up to 10 times) under UV light irradiation for 3 h

$$(H_2O \text{ or } OH^-) + h^+ \rightarrow OH^\circ + H^+ \quad (5)$$

$$O_2^{\circ-} + H^+ \rightarrow OH^\circ \quad (6)$$

$$\text{IC dye} + OH^\circ \rightarrow \text{intermediates} \rightarrow H_2O + CO_2 + NO_3^- + SO_4^{2-} \quad (7)$$

3.5 Reusability and stability of TNR hybrid sheets

The recovery and reuse of photocatalysts are another two crucial factors for the economically wastewater treatment process. The 3D porous-structured TNR_5 wt% hybrid sheet was thus investigated for recyclability on the photodegradation of IC dye under UV light irradiation. Not only is this TNR sheet be easily separated from the system, it can also be repeatedly used 10 times without the loss of its efficiency as shown in Fig. 9. Moreover, after each use the sheet remained clean and required no cleaning for the next subsequent use. The photodegradation efficiencies of the TNR sheet remained higher than 98% throughout the recyclability tests. Note that the efficiency of the first use was slightly lower than those of the subsequent uses, which is similar to the previously reported as attributing to the lower trace impurity on the sheet surface [30–32].

To evaluate the stability of this catalyst, the used TNR hybrid sheet was analyzed by the XRD and SEM techniques, respectively. Figure 10 displays the XRD patterns of TNR sheet before and after the 10th use, where all the key characteristic peaks of the sheet after having been used 10 times are still similar to the sheet prior use. This indicates that the sheet has high stability and retained its high efficiency up to the 10th use for the photodegradation of IC dye solution. However, on a close inspection, the peak intensity of natural rubber (a large broad peak near $2\theta = 19°$) of the sheet after the 10th use (see in Fig. 10b) has slightly lower intensity than the freshly prepared sheet (see in Fig. 10a). The slightly decrease of the relative intensity of the rubber characteristics on the sheet surface could due to the fact that during the first use, trace of impurities covering on the sheet surface were released in the photodegradation process; hence, after the first use, the sheet surface appeared to be cleaner. Furthermore, the loss of such an impurity whereas TiO_2 particles still remain impregnating on the sheet surface could expose the TiO_2 to the IC solution. In addition, the SEM images of the surface morphologies of TNR sheets before and after the 10th use were analyzed as shown in Fig. 11 to study the stability of the sheet surface. The surface morphology of the sheet after 10 use (see in Fig. 11b) showed sign of wearing out slightly,

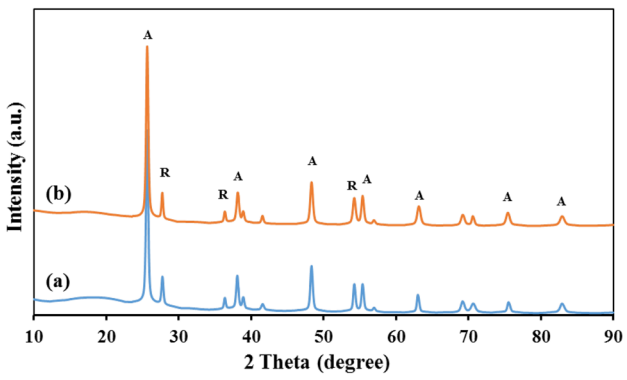

Fig. 10 XRD patterns of the 3D porous-structured TNR_5 wt% hybrid sheet: (a) before use (freshly prepared) and (b) after the 10th use

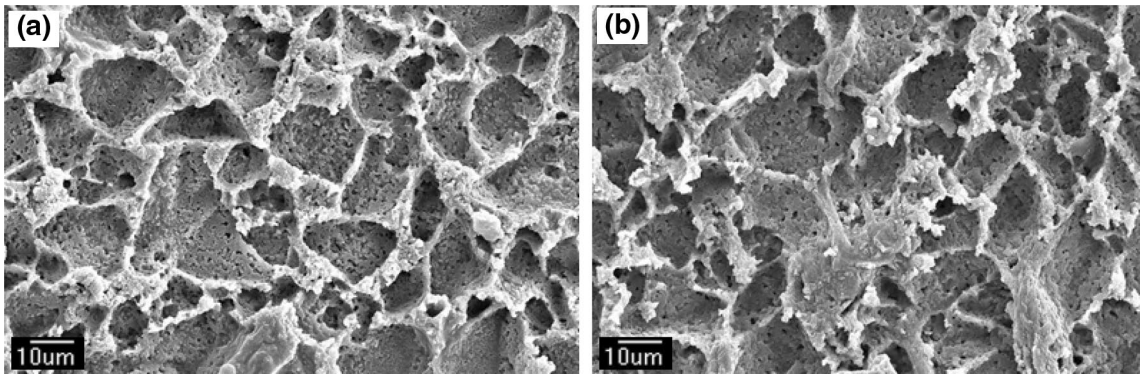

Fig. 11 SEM images of 3D porous-structured TNR_5 wt% hybrid sheet surface: **a** before use (freshly prepared) and **b** after the 10th use

especially at the edges of the thin walls of the 3D network structure when compared with the prepared sheet prior use (see in Fig. 11a). Nevertheless, this deterioration shows no significant effect on the photodegradation of IC dye as it still maintains high efficiency consistently until the end of 10 times of uses (see in Fig. 9).

4 Conclusion

In summary, we have successfully prepared the 3D porous network structured TNR sheet embedded with TiO_2 nano-photocatalyst using a simple and low cost method. The as-prepared TNR hybrid sheets exhibit the high photocatalytic property of pristine TiO_2 nanoparticles by photodegrading IC dye solution under UV light irradiation. The SEM results showed that the TNR_5 wt% hybrid sheet had highly impregnated by TiO_2 nanoparticles content, roughness, porosity, and 3D network structured on the surface than the others. Thus, it showed the highest photocatalytic efficiency. Comparing with the sheets in previous works, this 3D porous-structured TNR hybrid sheet had the better photodegradation of IC dye. Even though, the TNR sheet appears to be less efficiency than the loose powder of TiO_2, it has one promising advantage on the easily use as well as recovery after the use. Interestingly, it can be reused 10 times without the loss of its photodegradation efficiency with remained higher than 98%.

Acknowledgements The authors would like to thank the Faculty of Science, King Mongkut's Institute of Technology Ladkrabang for the financial support.

Compliance with ethical standards

Conflict of interest The authors declare that they have no conlict of interest.

References

1. Abu Bakar NH, Ismail J, Abu Bakar M (2007) Synthesis and characterization of silver nanoparticles in natural rubber. Mater Chem Phys 104:276–283
2. Asilturk M, Sener S (2012) TiO_2-activated carbon photocatalysts: preparation, characterization and photocatalytic activities. Chem Eng J 180:354–363
3. Ao Y, Xu J, Fu D, Yuan C (2008) Preparation of porous titania thin film and its photocatalytic activity. Appl Surf Sci 255:3137–3140
4. Ao Y, Xu J, Fu D, Shen X, Yuan C (2008) Low temperature preparation of anatase TiO_2-activated carbon composite film. Appl Surf Sci 254:4001–4006
5. Barrocas B, Monteiro OC, Melo Jorge ME, Serio S (2013) Photocatalytic activity and reusability study of nanocrystalline TiO_2 films prepared by sputtering technique. Appl Surf Sci 264:111–116
6. Chen F, Yang X, Wu Q (2009) Antifungal capability of TiO_2 coated film on moist wood. Build Environ 44:1088–1093
7. Elfeky SA, Al-Sherbini A (2011) Photocatalytic deposition of Trypan Blue over nanocomposite thin films. Kinet Catal 52(3):391–396
8. Filice S, Compagnini G, Fiorenza R, Scire S, D'Urso L, Fragala ME, Russo P, Fazio E, Scalese S (2017) Laser processing of TiO_2 colloids for en enhanced photocatalytic water splitting activity. J Colloids Interface Sci 489:131–137
9. Fostier AH, Pereira MSS, Rath S, Guimaraes JR (2008) Arsenic removal from water employing heterogeneous photocatalysis with TiO_2 immobilized in PET bottles. Chemosphere 72:319–324
10. Gu X, Xie D, Cao L, Du F (2014) Synthesis and characterization of TiO_2/ZrO_2 coaxial core-shell composite nanotubes for photocatalytic applications. Ceram Int 40:12647–12653
11. Guidelli EJ, Ramos AP, Zaniquelli MED, Baffa O (2011) Green synthesis of colloidal silver nanoparticles using natural rubber latex extracted from *Hevea brasiliensis*. Spectrochim Acta Part A 82:140–145
12. Ilinoiu EC, Pode R, Manea F, Colar LA, Jakab A, Orha C, Ratiu C, Lazau C, Sfarloga P (2013) Photocatalytic activity of a nitrogen-doped TiO_2 modified zeolite in the degradation of Reactive Yellow 125 azo dye. J Taiwan Inst Chem Eng 44:270–278
13. Juang RS, Chen CH (2014) Comparative study on photocatalytic degradation of methomyl and parathion over UV-irradiated TiO_2 particles in aqueous solution. J Taiwan Inst Chem Eng 45:989–995
14. Kasanen J, Suvanto M, Pakkanen TT (2011) Improved adhesive of TiO_2-based multilayer coating on HDPE and characterization of photocatalysis. J Appl Polym Sci 119:2235–2245

15. Kwon CH, Shin H, Kim JH, Choi WS, Yoon KH (2004) Degradation of methylene blue via photocatalysis of titanium dioxide. Mater Chem Phys 86:78–82
16. Langlet A, Kim A, Audier M (2002) Sol–gel preparation of photocatalytic TiO_2 films on polymer substrates. J Sol-Gel Sci Technol 25:223–234
17. Lee CS, Kim JW, Son JY, Choi W, Kim H (2009) Photocatalytic functional coatings of TiO_2 thin films on polymer substrate by plasma enhanced atomic layer deposition. Appl Catal B Environ 91:628–633
18. Li X, Wang D, Cheng G, Luo Q, An J, Wang Y (2008) Preparation of polyaniline-modified TiO_2 nanoparticles and their photocatalytic activity under visible light illumination. Appl Catal B Environ 81:267–273
19. Luan J, Chen M, Hu W (2014) Synthesis, characterization and photocatalytic activity of new photocatalyst $ZnBiSbO_4$ under visible light irradiation. Int J Mol Sci 15:9459–9480
20. Marcos PS, Marto J, Trindade T, Labrincha JA (2008) Screen-printing of TiO_2 photocatalytic layers on glazed ceramic tiles. J Photochem Photobiol A Chem 197:125–131
21. Mragui AE, Daou I, Zegaoui O (2019) Influence of the preparation method and ZnO/((ZnO + TiO_2) weight ratio on the physicochemical and photocatalytic properties of ZnO–TiO_2 nanomaterials. Catal Today 321–322:41–51
22. Nakata K, Fujishima A (2012) TiO_2 photocatalysis: design and applications. J Photochem Photobiol C Photochem Rev 13:169–189
23. Nawi MA, Zain SMd (2012) Enhancing the surface properties of the immobilized Degussa P-25 TiO_2 for the efficient photocatalytic removal of methylene blue from aqueous solution. Appl Surf Sci 258:6148–6157
24. Noorimotlagh Z, Kazeminezhad I, Jaafarzadeh N, Ahmadi M, Ramezani Martinez SS (2018) The visible-light photodegradation of nonylphenol in the presence of carbon-doped TiO_2 with rutile/anatase ratio coated on GAC: effect of parameters and degradation mechanism. J Hazard Mater 350:108–120
25. Oveisi M, Asli MA, Mahmoodi NM (2018) MIL-Ti metal–organic frameworks (MOFs) nanomaterials as superior adsorbents: synthesis and ultrasound-aided dye adsorption from multicomponent wastewater systems. J Hazard Mater 347:123–140
26. Qin X, Jing L, Tian G, Qu Y, Feng Y (2009) Enhanced photocatalytic activity for Degrading Rhodamine B solution of commercial Degussa P25 TiO_2 and its mechanisms. J Hazard Mater 172:1168–1174
27. Rathnayake IU, Ismail H, De Silva CR, Darsanasiri ND, Bose I (2015) Antibacterial effect of Ag-doped TiO_2 nanoparticles incorporated natural rubber latex foam under visible light conditions. Iran Polym J 24:1057–1068
28. Silva VS, Paschoalino PM, Goncalves MC, Felisberti MI, Jardim WF, Yoshida IVP (2009) Silicone rubbers filled with TiO_2: characterization and photocatalytic activity. Mater Chem Phys 113:395–400
29. Singh S, Mahalingam H, Singh PK (2013) Polymer-supported titanium dioxide photocatalyst for environmental remediation. Appl Catal A Gen 462–463:78–195
30. Sriwong C, Wongnawa S, Patarapaiboolchai O (2008) Photocatalytic activity of rubber sheet impregnated with TiO_2 particles and its recyclability. Catal Commun 9:213–218
31. Sriwong C, Wongnawa S, Patarapaiboolchai O (2012) Recyclable thin TiO_2-embedded rubber sheet and dye degradation. Chem Eng J 191:210–217
32. Sriwong C, Wongnawa S, Patarapaiboolchai O (2012) Rubber sheet strewn with TiO_2 particles: photocatalytic activity and recyclability. J Environ Sci 24(3):464–472
33. Sruanganurak A, Sanguansap K, Tangboriboonrat P (2006) Layer-by-layer assembled nanoparticles: a novel method for surface modification of natural rubber latex film. Colloids Surf A 289:110–117
34. Suwanchawalit C, Sriwong C, Wongnawa S (2010) Recyclable rubber sheets impregnated with potassium oxalate doped TiO_2 and their uses in decolorization of dye-polluted waters. Int J Environ Res 4(4):615–628
35. Valera-Zaragoza M, Yescas-Yescas A, Juarez-Arellano EA, Aguirre A, Aparicio-Saguilan A, Ramirez-Vargas E, Sepulveda-Guzman S, Sanchez-Valdes S (2014) Immobilization of TiO_2 nanoparticles on montmorillonite clay and its effect on the morphology of natural rubber nanocomposites. Polym Bull 71:1295–1313
36. Yang JH, Han YS, Choy JH (2006) TiO_2 thin-films on polymer substrates and their photocatalytic activity. Thin Solid Films 495:266–271
37. Yao PC, Hang ST, Lin CW, Hai DH (2011) Photocatalytic destruction of gaseous toluene by porphyrin-sensitized TiO_2 thin films. J Taiwan Inst Chem Eng 42:470–479
38. Yu G, Chen Z, Zhang Z, Zhang P, Jiang Z (2004) The photocatalytic activity and stability of a nanosized TiO_2 film prepared by carbon black modified method. Catal Today 90:305–312
39. Zhang X, Wang C, Yu C, Teng B, He Y, Zhao L, Fan M (2018) Application of Ag/AgBr/$GdVO_4$ composite photocatalyst in wastewater treatment. J Environ Sci 63:68–75
40. Zhan WT, Ni HW, Chen RS, Wang ZY, Li YW, Li JH (2013) One-step hydrothermal preparation of TiO_2/WO_3 nanocomposite films on anodized stainless steel for photocatalytic degradation of organic pollutants. Thin Solid Films 548:299–305